

## Two-plastic-hinge and two dimensional finite element models for post-tensioned precast concrete segmental bridge columns

Chung-Che Chou<sup>a,b,\*</sup>, Hao-Jan Chang<sup>c</sup>, Joshua T. Hewes<sup>d</sup>

<sup>a</sup> Department of Civil Engineering, National Taiwan University, Taipei, Taiwan

<sup>b</sup> National Center for Research on Earthquake Engineering, Taipei, Taiwan

<sup>c</sup> Department of Civil Engineering, National Chiao Tung University, Hsinchu, Taiwan

<sup>d</sup> Department of Civil and Environmental Engineering, Northern Arizona University, Flagstaff, AZ, USA

### ARTICLE INFO

#### Article history:

Received 11 October 2010

Revised 25 June 2012

Accepted 17 July 2012

Available online 13 September 2012

#### Keywords:

Precast concrete segmental bridge column

Unbonded strands

Cyclic tests

Two-plastic-hinge model

Finite element model

### ABSTRACT

Recent studies have confirmed that unbonded post-tensioned (PT) precast concrete segmental bridge columns are capable of undergoing large lateral deformation with negligible residual drift. To provide a clear guideline for the modeling of the columns for practicing engineers as well as researchers, this paper presents two types of numerical models: (i) a two-plastic-hinge model using the sectional moment–curvature analysis procedure at two segment interfaces and (ii) a two-dimensional (2D) finite element model using truss and beam–column elements in the computer program PISA. Three unbonded PT precast concrete-filled tube segmental bridge column specimens are cyclically tested. Two specimens have mild steel bars crossing to different column heights for studying the effects of anchorage position on the hysteretic energy dissipation (ED) capacity. The test results show that (1) the mild steel bars (“ED bars”) can increase hysteretic energy dissipation, and Specimens 1–3 have equivalent viscous damping of 6.5–8.8%, (2) a plastic hinge length in the first or second segment varies with anchorage position of ED bars and lateral displacement, and (3) an equivalent unbonded length along which the strain in the ED bar is assumed uniformly distributed on each of the two sides is 5–6 bar diameter. A 2D finite-element model is utilized to predict the cyclic behavior of the specimens. Parametric studies using finite-element models are also conducted to investigate the effects of ED bar area, initial strand force, and aspect ratio on the cyclic behavior.

© 2012 Elsevier Ltd. All rights reserved.

### 1. Introduction

Innovative precast concrete segmental bridge columns that incorporate unbonded post-tensioning elements to provide self-centering capacity and with devices to dissipate seismic input energy have recently been proposed in the United States as well as in other countries. Because of the limited knowledge regarding the seismic behavior of such columns, this type of bridge column has been used only in regions of low seismicity [1]. Hewes’s studies [2,3] confirmed that the columns are easily assembled in the laboratory and capable of undergoing large lateral deformations with small residual drift upon unloading, exhibiting a “flag-shaped” hysteretic behavior. The most significant characteristic of the behavior is bilinear-elastic but with hysteretic energy mainly added to the post-elastic portion of response. The resulting hysteretic energy dissipation capability is low in comparison with conventional monolithic reinforced concrete columns or concrete-filled tube columns [4]. Past studies showed that the addition of longitudinal mild steel bars crossing column segment joints or external steel plates at the column base can improve hysteretic energy dissipation capacity [5–7]. It has also been shown that incorporating ductility-dependent stiffness degradation in the flag-shaped hysteretic model can improve prediction of the columns subjected to seismic loads [8].

The lateral deformation of a PT segmental column is attributed primarily to gap opening at segment interfaces (joints). For convenience, it is assumed that the segmental column behaves like a conventional reinforced concrete column with a plastic hinge (gap opening) at the segment joint. Conventional moment curvature analysis, which is used to obtain the moment–rotation relationship of the self-centering connections [9,10], can be used to obtain the pushover curve of the segmental column [3,11]. However, when segment joints have unequal strengths, the pushover response of the segmental column cannot be determined based on a single plastic hinge at the column base. For a PT segmental

etic energy dissipation capability is low in comparison with conventional monolithic reinforced concrete columns or concrete-filled tube columns [4]. Past studies showed that the addition of longitudinal mild steel bars crossing column segment joints or external steel plates at the column base can improve hysteretic energy dissipation capacity [5–7]. It has also been shown that incorporating ductility-dependent stiffness degradation in the flag-shaped hysteretic model can improve prediction of the columns subjected to seismic loads [8].

\* Corresponding author at: Department of Civil Engineering, National Taiwan University, Taipei, Taiwan. Tel.: +886 2 3366 4349; fax: +886 2 2739 6752.

E-mail addresses: [cechou@ntu.edu.tw](mailto:cechou@ntu.edu.tw) (C.-C. Chou), [Joshua.Hewes@nau.edu](mailto:Joshua.Hewes@nau.edu) (J.T. Hewes).

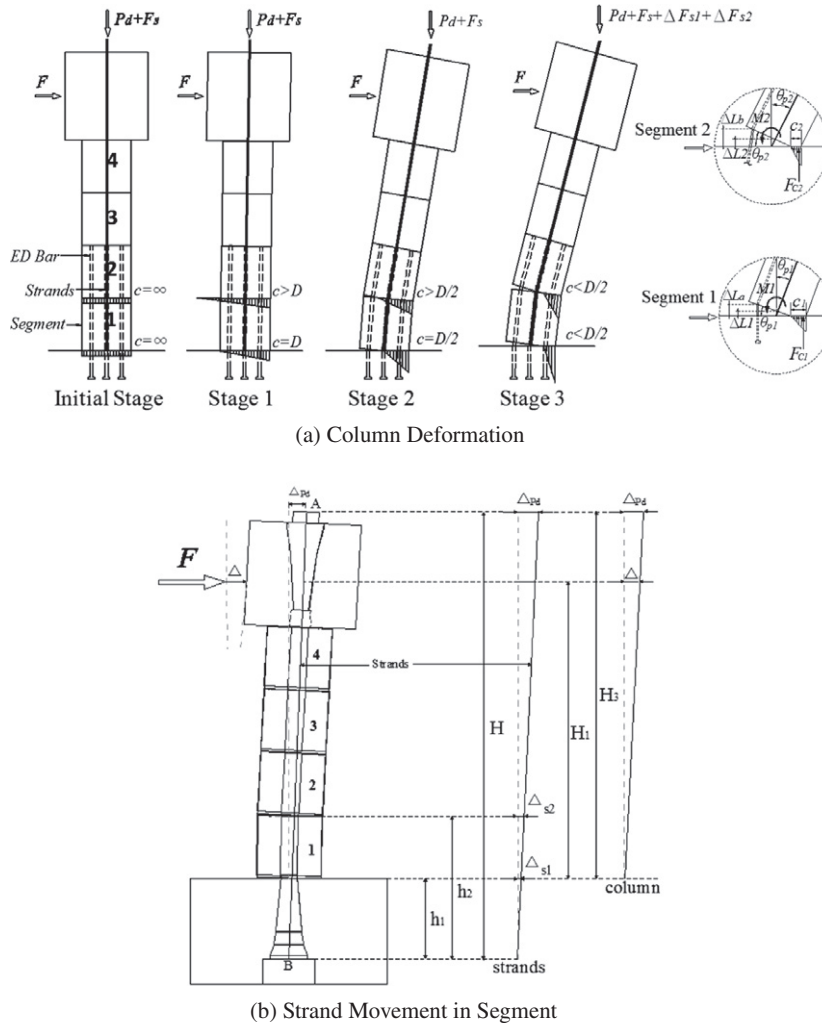


Fig. 1. Unbonded PT concrete segmental columns under lateral load.

column without energy dissipation devices at the base, the column lateral deformation can be characterized by rotation of the column about the bottom two segment interfaces and the corresponding lengths of two plastic hinges are [6]:

$$L_{p1} = 0.5d \quad (1)$$

$$L_{p2} = 0.2d \quad (2)$$

where  $L_{p1}$  is the plastic hinge length in the first segment;  $L_{p2}$  is the plastic hinge length in the second segment, and  $d$  is the cross-sectional diameter of the segmental column. Note that Eqs. (1) and (2) are obtained based on experimental curvatures along the column height, and a larger plastic hinge length is caused by a larger gap opening at the segment interface. Therefore, providing an energy dissipation device at the column base changes gap opening at segment interfaces and associated plastic hinge lengths.

This study extends the concept of “two plastic hinges” to develop an analytical model for predicting pushover responses of unbonded PT concrete segmental columns, where joint opening is mainly located at the bottom two segments. For verification purposes, cyclic tests were conducted on three columns. Each column segment was encased in a steel tube to raise the concrete compressive strength and ultimate compression strain. Two specimens included energy-dissipating (ED) bars with different

anchorage location for studying the effects of bar anchorage location on the plastic hinge length and energy dissipation. While Ou et al. [11] demonstrated that a detailed three-dimensional (3D) finite-element (FE) model utilizing solid elements in segments and contact elements between segment interfaces can predict the cyclic response of PT segmental columns in tests, this current work aimed instead to develop a simplified two-dimensional (2D) FE model using truss and beam-column elements to predict the cyclic behavior of PT segmental columns. This simpler modeling approach saves computation effort by reducing model complexity and serves as a reasonable alternative to 3D analyses. Based on the 2D FE model, a parametric study on unbonded PT concrete segmental columns was conducted to evaluate the optimum area and moment ratios of ED bars for a circular PT column section.

Table 1  
Material properties.

Specimen No.	Concrete (MPa)	Cement grout (MPa)	ED bar	
			Yield strength (MPa)	Tensile strength (MPa)
1	53	–	–	–
2	48	63	307	497
3	51	72	307	497

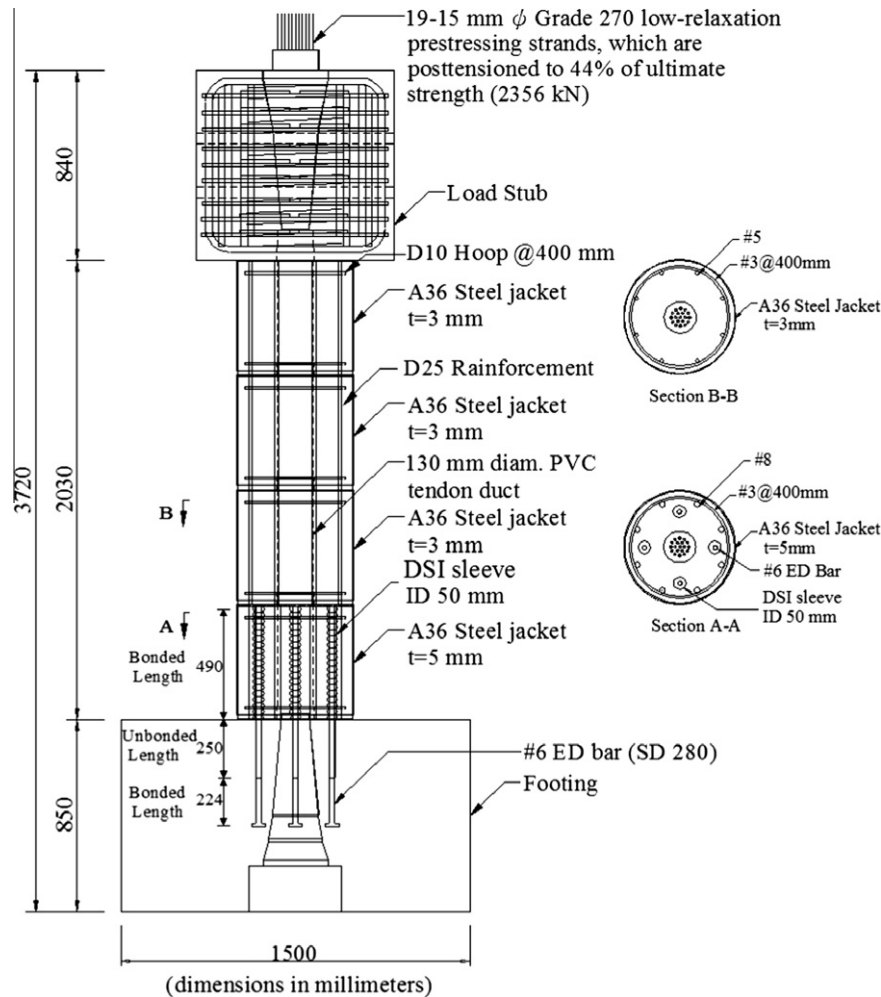


Fig. 2. Specimen 2 details.

## 2. Two-plastic-hinge model for precast concrete segmental bridge column

A PT concrete column is composed of a load stub, four segments and a footing, which are post-tensioned together by using unbonded strands (Fig. 1a). Eight longitudinal reinforcing bars (#8 and #5 reinforcement in the first and other segments, respectively) that do not cross segment joints are used to reduce compressive strains of concrete, while four ED bars are incorporated to increase energy dissipation of the column. The behavior of the unbonded PT concrete segmental column under a lateral load is characterized by three stages (Fig. 1a). Stage one corresponds to column response prior to decompression of the column at any section. Stage two commences when the PT force,  $F_s$ , begins increasing due to joint opening at the column base; a crack forms at the base and propagates to mid section depth. A crack also forms at the bottom of the second segment but does not reach mid depth, therefore not significantly affecting the strand elongation. This stage represents the beginning of significant nonlinearity in the pushover response. With a further decrease of the neutral axis depth within segments, the strand is stretched and the strand force increases. Stage three initiates when a crack at the bottom of the second segment propagates to mid section depth. The large opening of the first and second segment joints causes an increase of the PT force,  $\Delta F_{s1}$  and  $\Delta F_{s2}$ , respectively. The conventional moment–curvature analysis procedure proposed by Hewes and Priestley [3] can be applied to

obtain the pushover relationship of the column before stage three. A two-plastic-hinge model proposed in this study is then used to obtain the remainder of column response with an explicit accounting for opening at the bottom two segment joints. In this analysis, the tensile strength of concrete is set to zero to account for the effect of joint opening, and a linear strain distribution is assumed only for the regions in concrete compression zone.

ED bars that are continuous across lower segment joints are used to enhance the hysteretic energy dissipation. The unbonded portion of an ED bar is inserted into a tube to prevent buckling under compression, and the interior diameter of the tube slightly exceeds the diameter of the bar to allow for free axial deformation. The ends of an ED bar are bonded in the footing and a column segment. Elongation of the ED bar due to joint opening causes a uniform distribution of strain in the unbonded length, which penetrates into the bonded regions on both sides of the bar for a certain length. For simplicity, an additional unbonded length  $L_{ua}$  along which the strain in the bar is uniformly distributed is assumed on each of the two sides of the bar in the model. The value of  $L_{ua}$  was assumed to be one bar diameter ( $1d_b$ ) based on the research by Raynor et al. [12]. Bars tested by Raynor et al. [12] were confined by corrugated steel ducts with fiber reinforced grout, and the value of  $L_{ua}$  in this study was different for DYWIDAG corrugated ducts grouted with non-shrinkage high-strength cement. Moreover, no fibers were used to increase the tensile strength of grout, so the value of  $L_{ua}$  (5–6 bar diameter) obtained from this

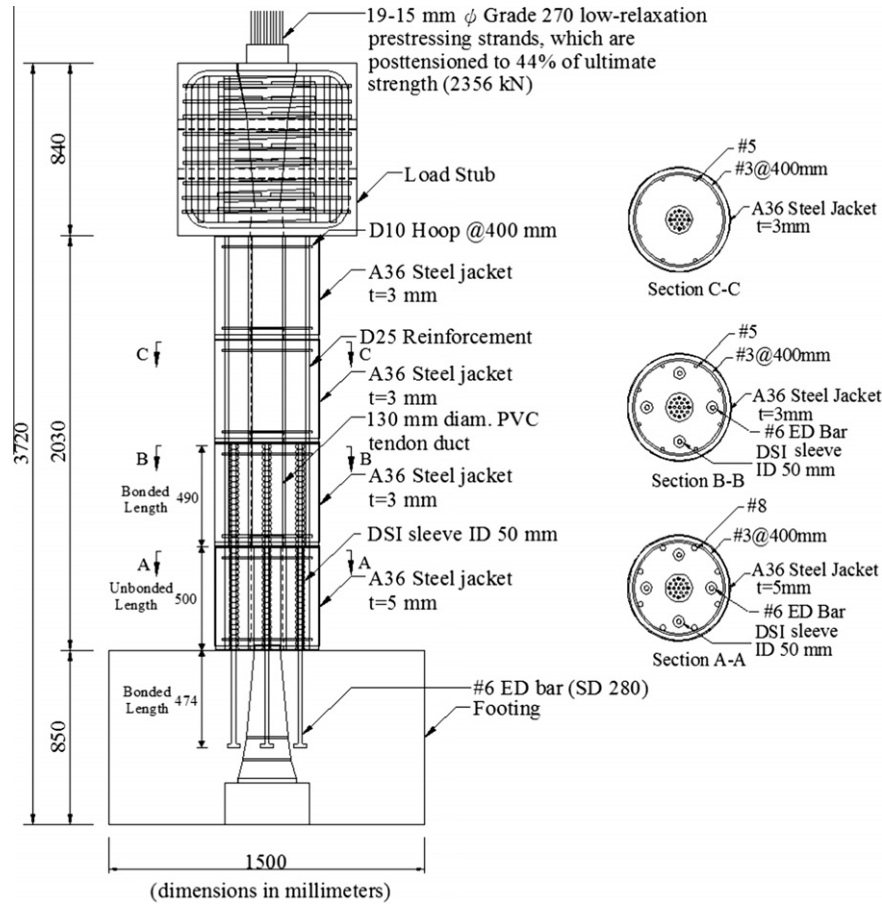


Fig. 3. Specimen 3 details.

**Table 2**  
Plastic hinge lengths of each specimen.

Specimen	1	2	3
$L_{p1}$	0.5d	0.5d	0.5d
$L_{p2}$	0.2d	0.5d	0.2d

### 2.1. Strand and ED bar strains

The change of strand axial force after decompression is a result of gap openings at the column base and the bottom of the second segment. Therefore, the tensile strain developed in the strands is:

$$\varepsilon_{st} = \varepsilon_{in} + \frac{1}{L} \left[ \theta_{p1} \left( \frac{D}{2} - c_1 \right) + \theta_{p2} \left( \frac{D}{2} - c_2 \right) \right] \quad (3)$$

where  $\theta_{p1}$  and  $\theta_{p2}$  are the angles of rotation in the first and second segments, respectively;  $c_1$  and  $c_2$  are the positions of the neutral axis at the column base and top of segment one, respectively;  $\varepsilon_{in}$  is the initial tensile strain in the strands, and  $L$  is the unbonded length of strands.

The tensile strain developed in the ED bar,  $\varepsilon_{ED}$ , is also a result of gap openings at the column base and bottom of segment two. The value of  $\varepsilon_{ED}$  is:

$$\varepsilon_{ED} = \frac{\Delta L_a + \Delta L_b}{L_{ED} + 2L_{ua}} = \frac{[\theta_{p1}d_1 + \theta_{p2}d_2]}{L_{ED} + 2L_{ua}} \quad (4)$$

where  $\Delta L_a$  is the elongation of the ED bar due to gap opening at the column base;  $\Delta L_b$  is the elongation of the ED bar due to gap opening at the bottom of segment two;  $L_{ED}$  is the unbonded length in the ED bar;  $d_1$  is the distance between the position of the ED bar and the neutral axis at the column base, and  $d_2$  is the distance between the position of the ED bar and the neutral axis at the bottom of segment two. If the ED bar is anchored in the first segment, the term  $\theta_{p2}d_2$  (and  $\Delta L_b$ ) in the numerator of Eq. (4) is omitted.

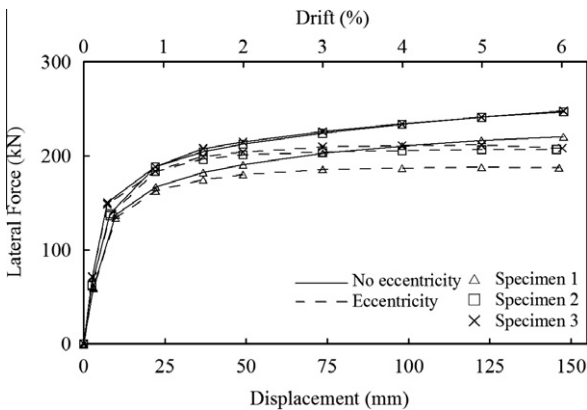


Fig. 4. Predicted pushover response based on the two-plastic-hinge model.

study was used, indicating that the non-shrinkage high-strength cement was not a good material in transferring bond forces. This value will be explained in the section of the test program.

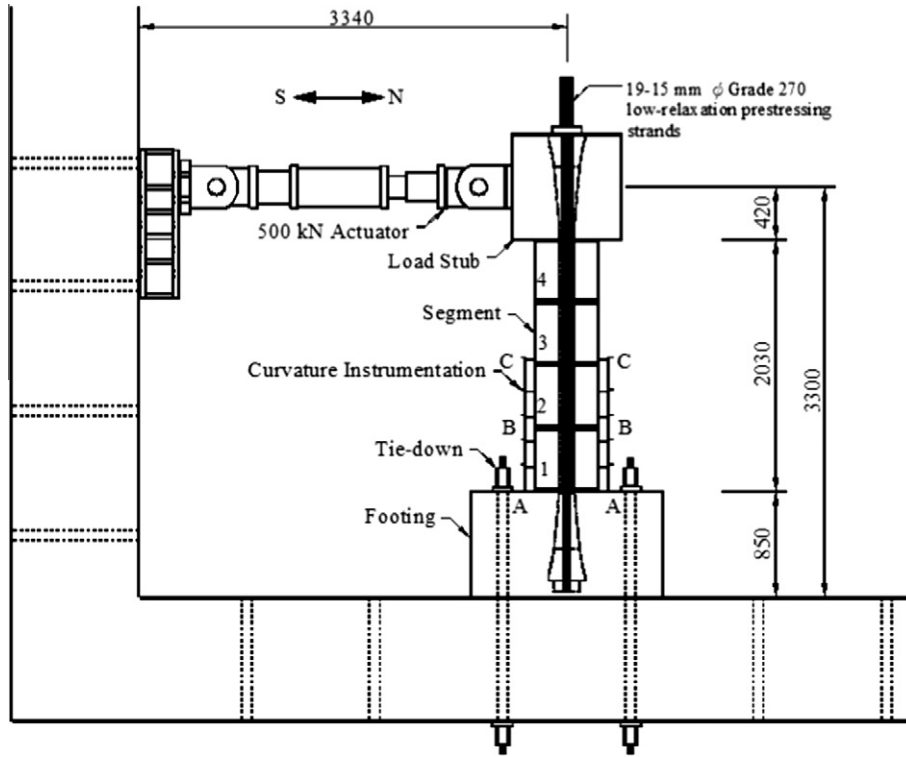


Fig. 5. Test setup.

## 2.2. Column lateral displacement

The column top flexural displacement,  $\Delta$ , can be expressed as

$$\Delta = \Delta_e + \Delta_{p1} + \Delta_{p2} \quad (5)$$

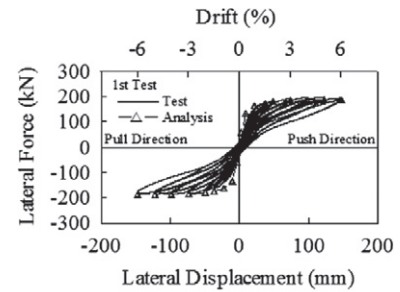
where  $\Delta_e$  is the elastic displacement of the column. The plastic displacement  $\Delta_{p1}$ , resulting from rigidly rotating the entire column about the column base, is expressed as

$$\Delta_{p1} = \left( \phi_b - \phi'_{y1} \frac{M_1}{M'_{y1}} \right) L_{p1} H_1 = \theta_{p1} H_1 \quad (6)$$

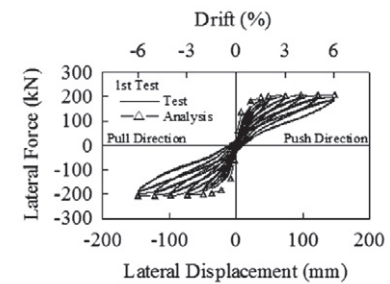
where  $L_{p1}$  is the plastic hinge length in the first segment (Eq. (1));  $\phi_b$  is the curvature at the base section;  $\phi'_{y1}$  is the theoretical “first yield” curvature at the base section, corresponding to the neutral axis position at the centroidal axis of the section;  $M'_{y1}$  is the theoretical “first yield” moment at the base;  $M_1$  is the computed moment at the base, and  $H_1$  is the height between the column base and the point of lateral loading. The column above segment one further rotates about the interface at the bottom of segment two, resulting in an additional plastic displacement  $\Delta_{p2}$ :

$$\Delta_{p2} = \left( \phi_2 - \phi'_{y2} \frac{M_2}{M'_{y2}} \right) L_{p2} H_2 = \theta_{p2} H_2 \quad (7)$$

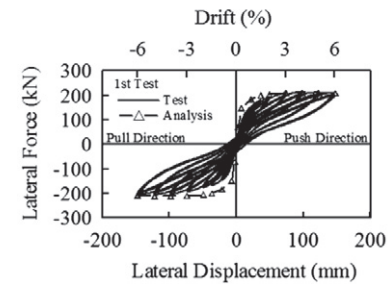
where  $L_{p2}$  is the plastic hinge length in the second segment (Eq. (2));  $\phi_2$  is the curvature at the bottom of segment two;  $\phi'_{y2}$  is the theoretical “first yield” curvature at the bottom of segment two, corresponding to the neutral axis position at the centroidal axis of the section;  $M'_{y2}$  is the theoretical “first yield” moment at the bottom of segment two,  $M_2$  is the computed moment at the bottom of segment two; and  $H_2$  is the height between the bottom of segment two and the point of lateral loading.



(a) Specimen 1



(b) Specimen 2



(c) Specimen 3

Fig. 6. Hysteretic response of unbonded PT concrete segmental columns.

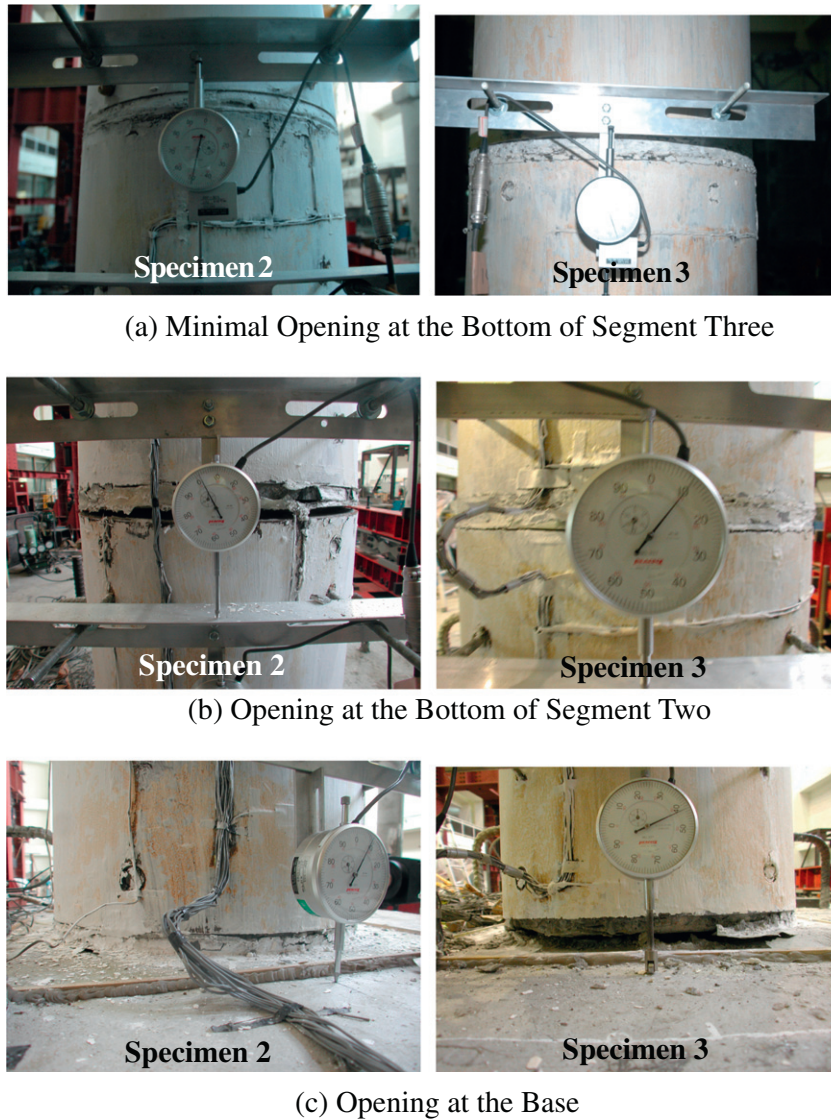


Fig. 7. Segment interface opening (6% drift).

### 2.3. Iterative procedure

The position of the neutral axis and the concrete extreme fiber compressive strain at the two interfaces are parameters to determine the angle of segment rotation, strand strain, ED bar strain and lateral displacement of the column. Thus, an iterative procedure has to be carried out in the calculation of the pushover response of the column. This can be done by applying the moment–curvature analyses at the two interfaces with increasing concrete compressive strain at the base. The tensile strength of concrete is set to zero to account for the effect of joint opening, and a linear strain distribution is assumed for concrete and longitudinal bars in compression. For a given concrete extreme fiber compressive strain  $\varepsilon_{c1}$  at the base of the column, at step  $n$ , the procedure to calculate the corresponding lateral displacement at the top of the column is described as follows. At an iteration  $i$ , knowing the lateral force  $F$  at an iteration  $i - 1$ , one can obtain the corresponding curvature at each interface by interpolating the moment–curvature analysis:

1. Assume a position of the neutral axis,  $c_1$ , at the column base, a position of the neutral axis,  $c_2$ , and the concrete extreme fiber compressive strain,  $\varepsilon_{c2}$ , at the bottom of segment two.
2. Calculate the angle of rotation  $\theta_{p1}$  and  $\theta_{p2}$  based on the respective plastic hinge length and the linear normal strain profile in the compression zone characterized by the concrete extreme fiber compressive strain and zero strain at the neutral axis at each interface.
3. Compute the tensile strain  $\varepsilon_{st}$  in the strands, the tensile strain  $\varepsilon_{ED}$  in the ED bars, and the compressive strain in the longitudinal reinforcement in the segment.
4. Compute the resulting normal stresses using the individual stress–strain relationships for each of the components. The concrete compressive stress is computed based on the confined concrete model proposed by Mander et al. [13]. The stress in the longitudinal reinforcement and the ED bar are calculated based on a bi-linear steel stress–strain relationship.
5. Integrate the normal stresses over the respective areas to obtain the corresponding normal force in each component.
6. Sum the normal forces; check for vertical force equilibriums at the base and the interface above segment one, respectively, and the ratio of computed moment  $M_1/M_2 (=H_1/H_2)$ . The ratio of  $M_1/M_2$  is always constant since  $H_1$  and  $H_2$  do not vary throughout loading.
7. Iterate over the positions of the neutral axis and concrete compressive strain by returning to step 1 until two vertical force equilibriums and one moment ratio are satisfied.

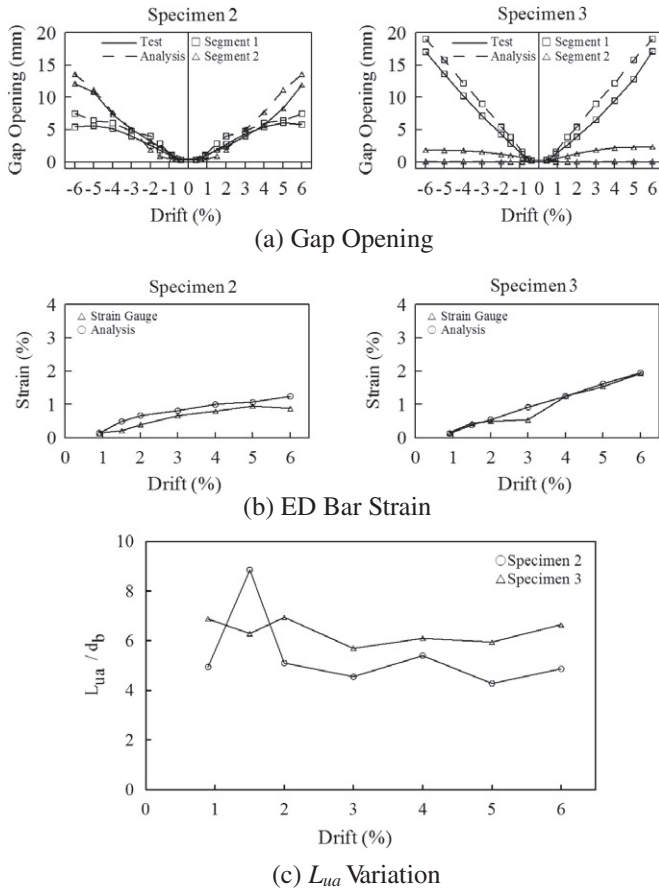


Fig. 8. Comparison between test and analysis.

8. The lateral force,  $F$ , is then updated based on the moment at the column base. The iterations are continued until the lateral forces,  $F$ , in two consecutive iterations are close (within 5% difference). The column top displacement is then calculated using Eqs. (5)–(7).

The procedure is repeated for increasing values of the concrete extreme fiber compressive strain at the base until the complete pushover relationship is determined. Termination of the analysis occurs when the confined concrete compressive strain reaches the ultimate strain  $\epsilon_{cu}$  [13]. The maximum axial strain in the ED bar is limited to 12 times the yield strain, which is about 2%. This strain level is much less than the fracture strain of ASTM A615M Grade 40 (280) reinforcement [14]. The past study [15] also showed that the ED bar within the strain limit of 2% sustained many cycles of inelastic loading before fracture. As long as the strain limit (2%) was adopted, the Grade 60 steel performed as well as the Grade 40 steel. Fracture of the PT strands did not occur prior to the failure of concrete due to the use of unbonded strands. Based on past studies on PT structural systems [15–19], a maximum strand force limited to 70–80% of the ultimate strand force prevented fracture of strands. The maximum strand force in this study was conservatively limited to  $0.5f_{pu}A_{st}$  where  $A_{st}$  is the area of the strands and  $f_{pu}$  (=1860 MPa) is the ultimate tensile strength of the strand. A conservative value, 50% of the ultimate, was adopted in this study to maintain the same PT load as Specimen 1, which was previously tested [6].

Note that in the development of the pushover curve, the strand is assumed at the center of segment interfaces. However, as the top of the column displaces  $\Delta$ , the position of strands moves away

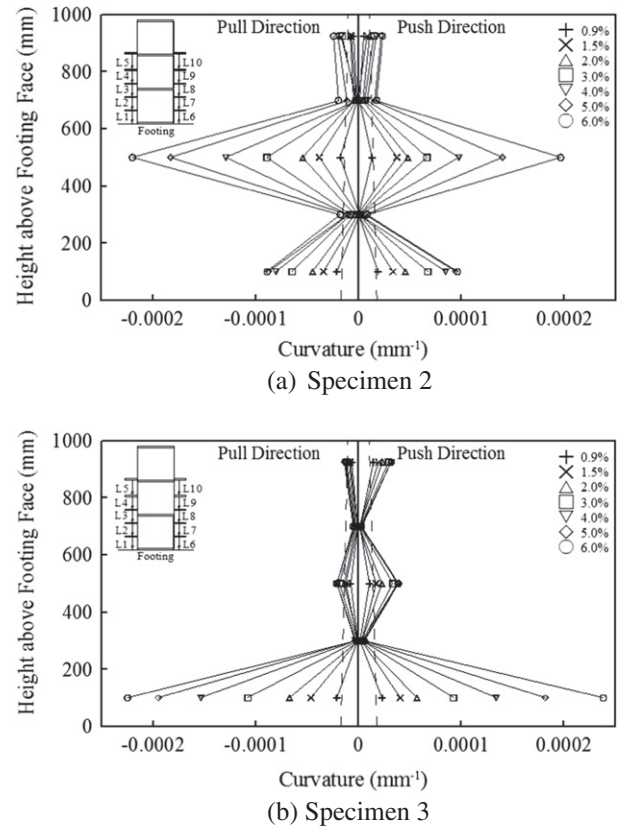


Fig. 9. Curvature along column height.

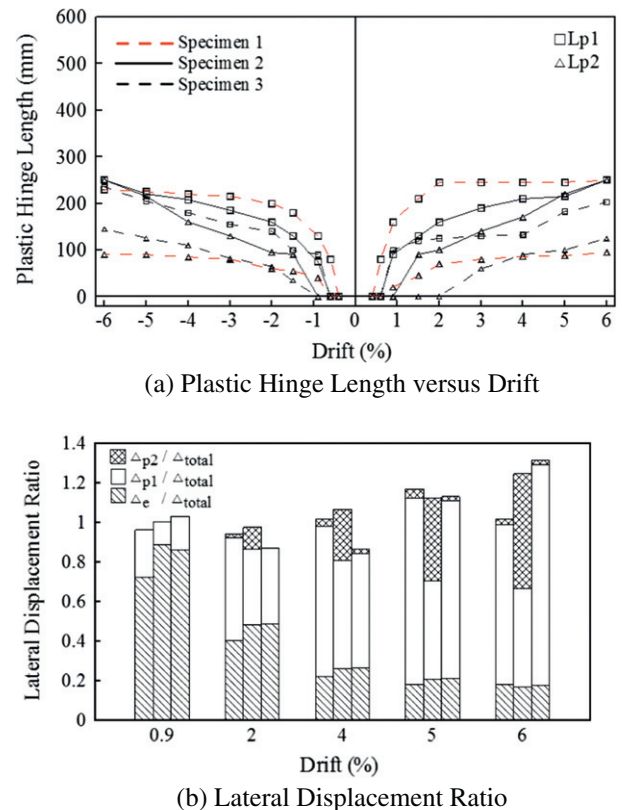


Fig. 10. Plastic hinge length and lateral displacement ratio (experimental results).

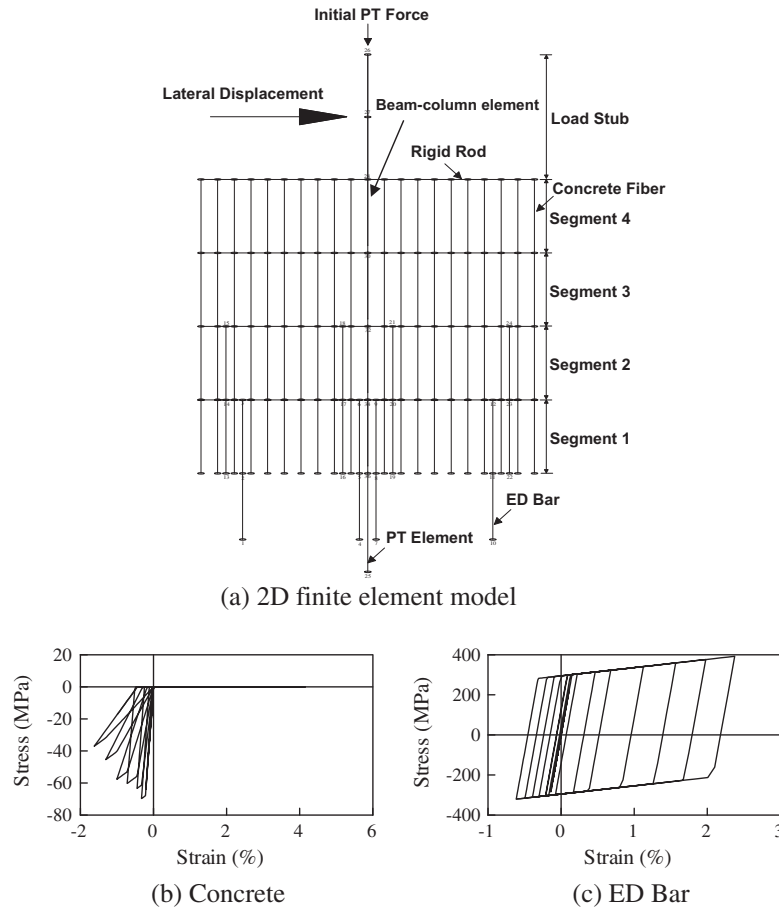


Fig. 11. Finite element model for an unbonded PT precast concrete segmental column.

from the segment center (Fig. 1b) with strands anchored in the load stub (point A) and the footing (point B). Assuming a linear deformed shape of strands between the points A and B, the displacements of strands at the bottom two joints are given by:

$$\Delta_{s1} = \frac{\Delta H_3}{H_1 H} h_1 \quad (8)$$

$$\Delta_{s2} = \frac{\Delta H_3}{H_1 H} h_2 - (\theta_{p1} h_s) \quad (9)$$

where  $H$  is the height between the top and bottom strand anchorages;  $h_1$  is the height between the bottom strand anchorage and the column base;  $h_2$  is the height between the bottom strand anchorage and the bottom of segment two;  $H_3$  is the height of the top strand anchorage measured from the column base, and  $h_s$  is the segment height. Since the column top displacement  $\Delta$  affects the position of strands in segments, a modification of the iterative procedure has to be carried out after obtaining the displacement of the column. Repeat the iterative procedure from step 3 using the updated position of strands to find out the updated strand force, moment, and column top displacement,  $\Delta$  (Eq. (5)). The iterations are continued until the difference between two consecutive iterations in terms of  $\Delta$  is sufficiently small.

### 3. Experimental program

#### 3.1. Specimen details

The experimental program [20] had three unbonded PT precast concrete segmental bridge columns which had a footing, four

concrete-filled tube (CFT) segments, and a load stub. Each column was post-tensioned with nineteen 15-mm diameter seven wire, uncoated, low-relaxation ASTM A416 Grade 270 strands placed at the mid-depth of the cross section. The total initial PT force after losses was 2365 kN, 2321 kN and 2300 kN for Specimens 1, 2 and 3, respectively. Specimen 1 was previously tested by Chou and Chen [6], and Specimens 2 and 3 were tested in this study. The specimens were identical except that Specimens 2 and 3 had a total of four #6 ED bars to enhance hysteretic energy dissipation and eight longitudinal reinforcing bars in the segments (but not across segment joints) to reduce concrete compressive strains. The ratio of the area of ED bars to concrete sectional area was  $\rho = 0.66\%$ . The ED bars conformed to ASTM A615M Grade 40 (280) steel reinforcement (Table 1) and each had a circular steel plate welded on one end, which was anchored in the footing. For Specimen 2 (Fig. 2), the other end of the ED bar was bonded in the first segment using high-strength non-shrinkage grout (Table 1). The bonded length was 490 mm, larger than 380 mm specified in Section 6.5.1 of PCI Design Handbook [21]. The upper end of ED bars in Specimen 3 was anchored in the second segment (Fig. 3). Note that the maximum strain in the ED bars depends on not only the unbonded length but also the location of bar anchorage. Elongation of ED bars in Specimen 3, which is caused by joint opening at the base and the interface above the first segment, is much larger than that in Specimen 2, which is caused by joint opening at the base only. Although the unbonded lengths of ED bars were 250 and 500 mm in Specimens 2 and 3, maximum tensile strains of Specimens 2 and 3 were 1.2% and 2.1%, respectively, at a 6% drift.

Table 2 lists plastic hinge lengths of each specimen in the analysis. Because the ED bars in Specimen 2 were anchored in the first

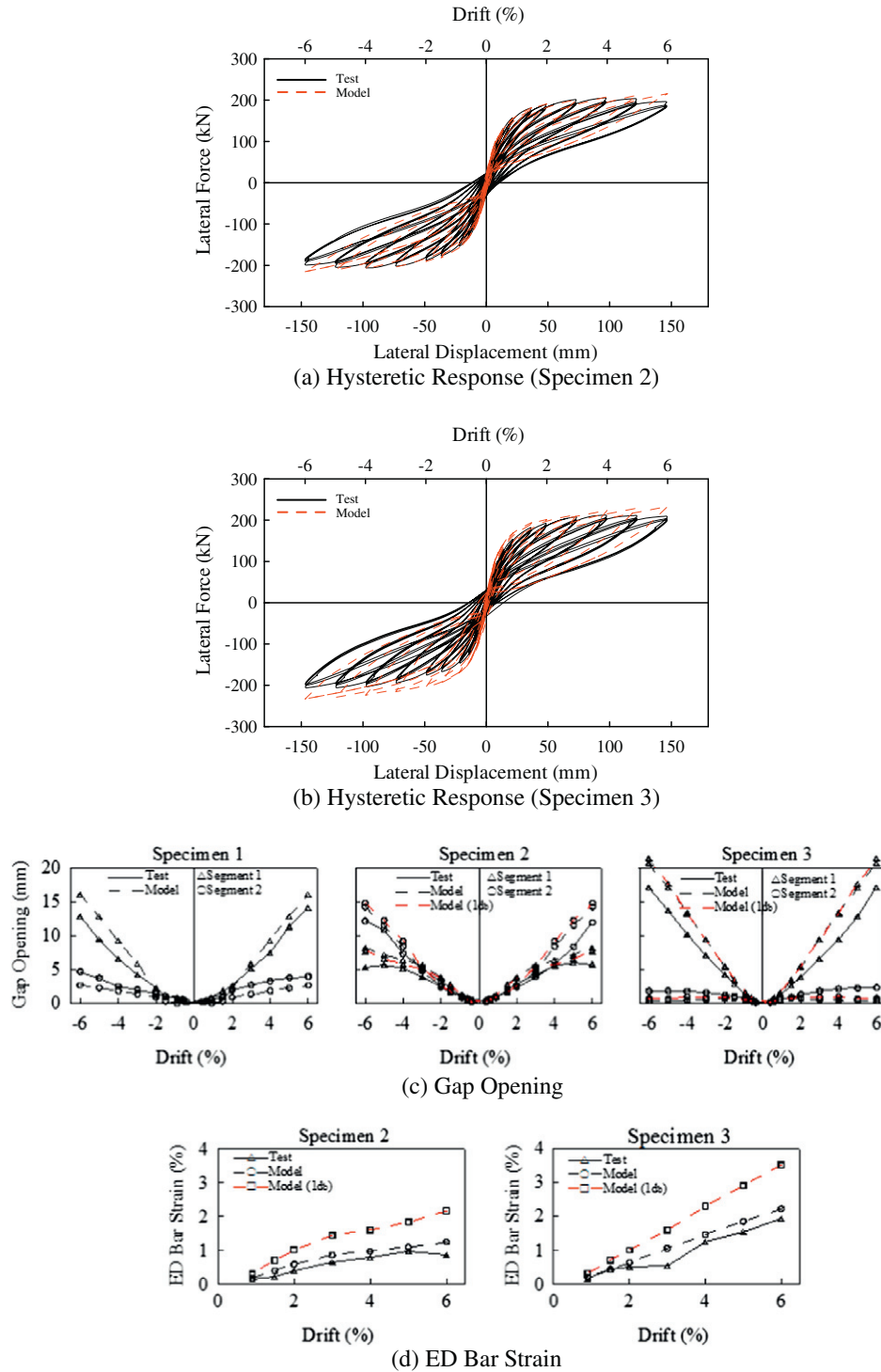


Fig. 12. Experimental validation of a FE model for a PT precast concrete segmental column.

segment, thus increasing the fixity of the first segment and leading to large column lateral deformations with respect to the interface at the top of segment one,  $L_{p2} = 0.5d$  was used instead of Eq. (2). Plastic hinge lengths were obtained based on the test conducted earlier for similar PT precast concrete segmental bridge columns [6]. The plastic hinge length, which is defined as the region where the experimental curvature is larger than the ideal yield curvature when the column is under lateral loading, increases with drift and approximates to certain values in segments one and two after 3% drift (Table 2). These values listed in Table 2 might apply for only the type of columns in this study and might change for columns

with different height-diameter ratio, column shape, and initial PT stress in the cross-sectional area. Fig. 4 shows the predicted push-over response of three specimens based on the two-plastic-hinge model; the peak strength when considering the eccentricity of strands is lower than that without considering strand eccentricity.

### 3.2. Test setup

A 500-kN actuator was placed at the load stub (Fig. 5), and the specimen was then tested quasi-statically with a pre-defined displacement history, consisting of one drift cycle with amplitudes

of 0.1%, 0.15%, 0.2%, and 0.3%, followed by three drift cycles with amplitudes of 0.4%, 0.6%, 0.9%, 1.5%, 2%, 3%, 4%, 5%, and 6%. Since the ultimate concrete compression strain calculated based on the confined concrete model [13] was 0.029, which was exceeded when the column drift was 6%, the test was stopped after completing two cycles at a drift of 6%.

### 3.3. Results of experiments

Fig. 6 shows the hysteretic response of three specimens during the test. The peak strengths are close to the predicted values as seen in the figure. Hysteretic energy dissipation of Specimen 1 was associated with the plastic straining of concrete in compression, and that of Specimens 2 and 3 were associated with the plastic straining of the ED bar and of concrete in compression. The hysteretic energy increased slightly with drift, and the equivalent viscous damping [22] for Specimens 2 and 3 at a 6% drift were 7.5% and 8.8%, higher than 6.5% of Specimen 1 at the same drift. Fig. 7 shows the opening of segment joints for Specimens 2 and 3 in the test. The joint opening at the bottom of segment three (Fig. 7a) was small compared to that of bottom two segments (Fig. 7b and c). Although the gap at the base of Specimen 3 was very large, ED bar buckling or fracture was not observed during the test. This can be confirmed by stable hysteretic responses of Specimen 3 throughout the test (Fig. 6c). For Specimen 2 with ED bars anchored at the footing and segment one, opening at the bottom of segment two was larger than that at the column base (Figs. 7 and 8a), leading to small elongation of ED bars. For Specimen 3 with ED bars anchored at the footing and segment two, a larger opening was observed at the column base than at the bottom of segment two throughout the test (Figs. 7 and 8a). Elongation of ED bars in Specimen 3 was primarily caused by joint opening at these two interfaces. Although the unbonded length of ED bars in Specimen 3 was double that in Specimen 2, the tensile strain of ED bars was larger in Specimen 3 than Specimen 2 (Fig. 8b). The maximum strain in the ED bar predicted by the two-plastic-hinge model shows agreement with that obtained from the tests. The value of  $L_{ua}$  on both sides of the original unbonded length was  $5d_b$  and  $6d_b$  in Specimens 2 and 3, respectively. These two values were determined by equating the strain gauge reading in the unbonded length of the ED bar to a strain value calculated based on elongation of the ED bar from the gap-opening angle and the position of the neutral axis during the tests. Fig. 8c shows variation of  $L_{ua}$ , approaching to a constant value ( $5-6d_b$ ) at a medium-to-high column drift.

Fig. 9 shows the distribution of curvature along the column height for both the push and pull directions. The experimental curvatures were calculated as

$$\phi = \frac{A_t - A_c}{DL_g} \quad (10)$$

where  $A_t$  is the elongation of a displacement transducer on the tension side of the segment;  $A_c$  is the shortening of a displacement transducer on the compression side of the segment at the same height level;  $D$  is the horizontal distance between these two displacement transducers, and  $L_g$  is the gage length. Note that the curvature at the column base and the bottom of segment two is larger than that at the bottom of segment three, indicating that joint opening is most significant at the bottom two joints. This is corresponding to the observed performance in the test (Fig. 7). Moreover, for Specimen 2, the gap opening at the base was smaller than that at the bottom of the second segment, leading to the curvature at the base smaller than that at the bottom of second segment. Stiffening of segment 2 in Specimen 3 was provided by the bonded ED bars, so

**Table 3**  
Comparison of the FM model prediction to the experimental response.

	Drift (%)						
	0.9	1.5	2	3	4	5	6
<i>Specimen 1</i>							
Model (kN)	147	164	171	183	196	202	202
Test (kN)	153	179	179	190	196	196	194
Ratio	0.96	0.92	0.96	0.96	1	1.03	1.04
<i>Specimen 2</i>							
Model (kN)	158	180	191	202	208	212	216
Test (kN)	155	178	187	200	204	201	194
Ratio	1.02	1.01	1.02	1.01	1.02	1.05	1.11
<i>Specimen 3</i>							
Model (kN)	171	194	202	214	224	229	233
Test (kN)	155	179	191	206	211	210	208
Ratio	1.1	1.08	1.06	1.04	1.06	1.09	1.12

the curvature of Specimen 3 (Fig. 9b) at the base was always larger than that at the bottom of the second segment.

The plastic hinge lengths  $L_{p1}$  and  $L_{p2}$  in segments 1 and 2 were calculated based on the method by Chou and Chen [6]. Fig. 10a shows that plastic hinge length increases with drift and approximates to half the section diameter in the first and second segments in Specimen 2. The plastic hinge length in Specimen 3 approximates to half the section diameter in first segment and one-fifth the section diameter in second segment, as observed in Specimen 1. This indicates that the anchorage position of ED bars affects the curvature in the plastic hinge region, the plastic hinge length in segments, the elongation of ED bars, and corresponding energy dissipation capacity. This is logical since stiffness is inversely proportional to curvature. The plastic hinge length, a constant value obtained at a high drift in each segment, was used for simplicity in the iterative procedure in predicting the pushover curve of columns. Fig. 6 shows the analytical results close to peak values of the hysteresis response of columns in the tests. Fig. 10b shows ratios of the flexural displacements  $\Delta_e$ ,  $\Delta_{p1}$ , and  $\Delta_{p2}$ , which were calculated based on experimental curvatures (Fig. 9) and plastic hinge lengths (Fig. 10a), to the imposed displacements  $\Delta_{total}$  by the actuator. Each drift has three bars: the first represents ratios of Specimen 1, while the second and third represent those of Specimens 2 and 3, respectively. The contribution of the flexural displacement due to the second segment rotation is small in Specimens 1 and 3. Except for the drift of 6%, the summation of measured displacements is close to the actuator displacement. Concrete at the base crushes at a drift of 6%, leading to more deformation measured by the displacement transducer placed in the concrete crush zone. Therefore, the curvature calculated at the base is overestimated and the associated displacement is larger than the test result.

## 4. Finite element analysis

A two-dimensional (2D) finite-element model for unbonded PT concrete segmental bridge columns was developed in this research. The model was created and analyzed using the computer program, PISA [23]. Different analytical models for investigating seismic performances of PT structures can be found elsewhere [24–26]. The modeling techniques of unbonded PT columns are described as follows and schematically illustrated in Fig. 11.

### 4.1. PT segmental column model

Fig. 11a illustrates a typical column model with four segments, each of which is composed of 50 concrete fibers. Each fiber is modeled using one dimensional truss element which consists of two nodes, each with three degrees of freedom: translations in the x and y-directions and rotation about the z-direction. The truss ele-

ments representing the segments are linked at segment joints with a number of horizontal rigid rods and are fixed at the footing interface. Two rigid rods extending from the top of the fourth segment represent the load stub. Considering that the shear demand at segment interfaces is significantly smaller than the friction capacity in the compressive area and that the truss elements do not transfer shear forces, a beam-column element with an effective shear area is used in the center of the section and is linked at each segment joint to transfer column shears. No flexural and axial stiffnesses are specified to the beam-column elements. The ultimate concrete compressive strength and strain are calculated based on Mander's confined concrete stress-strain model [13]. Degradation of the concrete under compressive cyclic loading is described using the three-parameter concrete model [27] in the computer program PISA. The three parameters in the model, which describes stiffness degradation, strength deterioration, and pinching of concrete under cyclic loading, are 10, 0.88, and 1.0, respectively. The concrete tensile strength and stiffness are assumed to be zero. Fig. 11b shows a typical response of a concrete truss element in cyclic loading.

The strands are modeled as a tension-only truss element (PT), which is anchored between the top of the load stub and bottom of the footing. The tensile force in the PT element increases when gap opening at segment interfaces extends beyond the center of the segment. Since the strands are within the elastic range in the tests, elastic behavior is assigned to the strands. Each ED bar has an unbonded length to dissipate seismic energy and a bonded length for anchorage. The bonded length of the ED bar is modeled as a rigid element and its end is anchored to the horizontal rigid rod at the segment interface. The other end of the ED bar is fixed to the base. The ED bar is loaded whenever the node of a horizontal rigid rod at the segment interface deforms relative to the base. The stress-strain response of the ED bar under cyclic loading is approximated by a bi-linear kinematic hardening model (Fig. 11c). Longitudinal reinforcement in the segment for reducing concrete compressive strain is modeled as a truss element with compression only properties.

#### 4.2. Verification of the FE model

The analysis was conducted in two steps to simulate the actual behavior of an unbonded PT concrete segmental column. The initial compressive force to the column from strands was applied by a preload at the top of the load stub. The column was then subjected to the applied lateral displacement at the centroid of the load stub and the corresponding lateral force was determined by the shear force developed in a rigid bar representing the load stub. Fig. 12a and b shows comparisons of the cyclic responses obtained from the FE models along with the experimental results of Specimens 2 and 3. The ratio of the FE model prediction to the experimental response is listed in Table 3. The response of the FE model is in good agreement with the cyclic response of the specimen within the target drift. The series of distributed concrete truss elements allows for measurement of the gap opening: the extension of the extreme concrete truss element in each segment reasonably predicts the gap opening at the segment interface (Fig. 12c). Because larger gap opening obtained from the FE model results in larger strains in the ED bars and PT strands, the peak strength predicted by the FE model is larger than that from the experimental response. The maximum strains in the ED bars predicted by the FE models show agreement with those obtained by Specimens 2 and 3 tests (Fig. 12d). Significant differences exist in the results in terms of the maximum ED bar strain when the equivalent unbonded length  $L_{ua}$  on each side of the original unbonded length of the ED bar is assumed as one bar diameter ( $1d_b$ ) in the model. However, the discrepancy of the gap-opening due to the assumption of one bar diameter in the model is minor (Fig. 12c).

#### 4.3. Parametric study

An analytical study using the modeling techniques described earlier was conducted for 24 unbonded PT segmental column models. Three parameters were investigated in this study: the aspect ratio, the amount of initial PT force, and ED bars. As listed in

**Table 4**  
Column model details.

Model No.	Column size			Segment number	Column height (mm)	Initial PT force			ED bar		
	Segment size		$A = 0.25f'_c A_c$			$B = 0.35f'_c A_c$	$\rho$ (%)	Unbonded length (mm)	Anchorage position (segment)	$\epsilon_{max}$ (%)	
Diameter (mm)	Height (mm)										
3	500	500	4	2450	A	2300	0.66	740	2	2.4	
4	500	500	4	2450	A	2300	1.2	740	2	2.4	
5	500	500	4	2450	A	2300	1.8	740	2	2.3	
6	500	500	4	2450	A	2300	2.4	740	2	1.9	
7	500	500	8	4900	A	2300	0.66	740	4	2.5	
8	500	500	8	4900	A	2300	1.2	740	4	2.5	
9	500	500	8	4900	A	2300	1.8	740	4	2.4	
10	500	500	8	4900	A	2300	2.4	740	4	2.0	
11	1000	1000	4	4900	A	9048	0.66	1480	2	2.5	
12	1000	1000	4	4900	A	9048	1.2	1480	2	2.4	
13	1000	1000	4	4900	A	9048	1.8	1480	2	2.4	
14	1000	1000	4	4900	A	9048	2.4	1480	2	2.0	
15	500	500	4	2450	B	3220	0.66	740	2	2.2	
16	500	500	4	2450	B	3220	1.2	740	2	2.2	
17	500	500	4	2450	B	3220	1.8	740	2	2.1	
18	500	500	4	2450	B	3220	2.4	740	2	1.5	
19	500	500	8	4900	B	3220	0.66	740	4	2.3	
20	500	500	8	4900	B	3220	1.2	740	4	2.3	
21	500	500	8	4900	B	3220	1.8	740	4	2.2	
22	500	500	8	4900	B	3220	2.4	740	4	1.9	
23	1000	1000	4	4900	B	12,667	0.66	1480	2	2.3	
24	1000	1000	4	4900	B	12,667	1.2	1480	2	2.4	
25	1000	1000	4	4900	B	12,667	1.8	1480	2	2.2	
26	1000	1000	4	4900	B	12,667	2.4	1480	2	1.9	

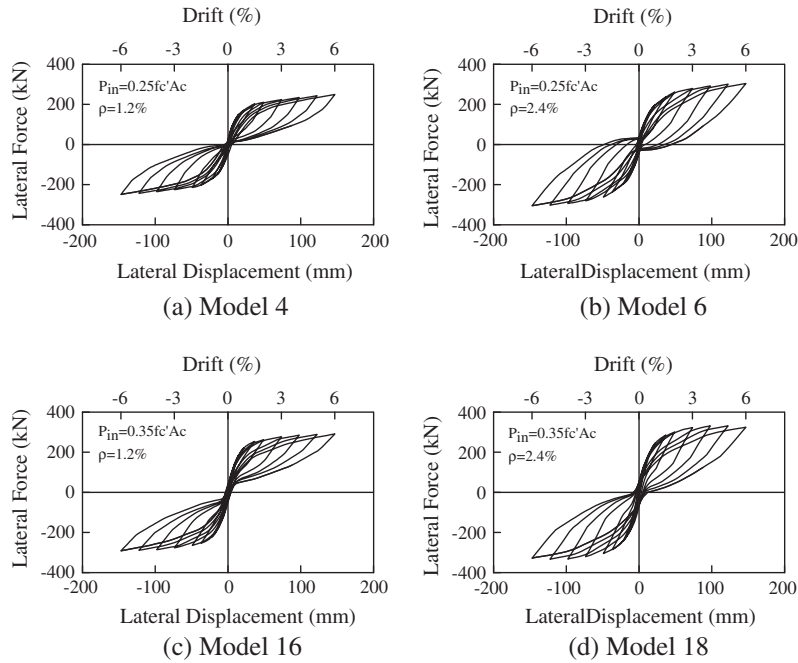
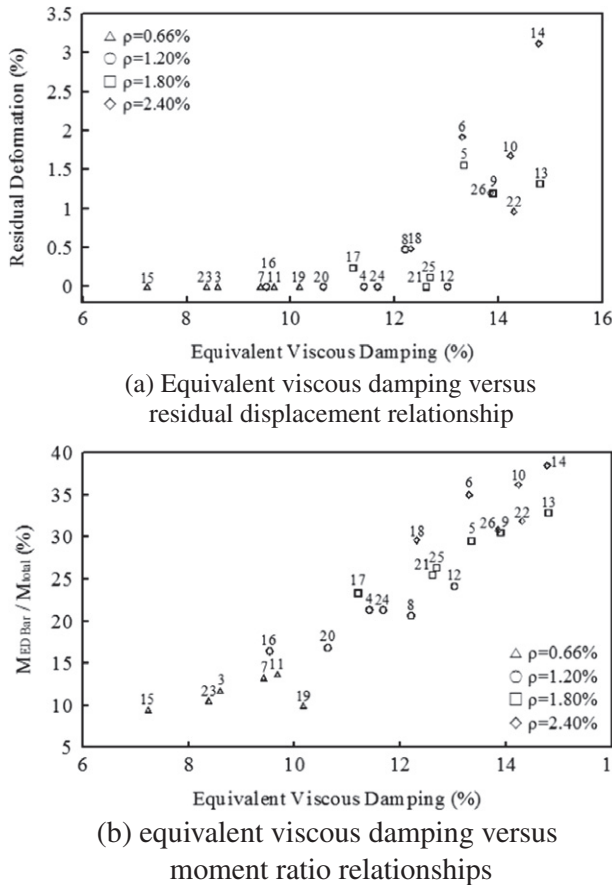


Fig. 13. Effects of ED bar ratio and PT force on cyclic behavior.



ratios of the area of ED bars to concrete sectional area  $A_c$  are  $\rho = 0.66\%$ ,  $1.2\%$ ,  $1.8\%$ , and  $2.4\%$ . The ED bar in this study is anchored at the base and the mid-height of the column and the maximum tensile strain in its unbonded length,  $\epsilon_{max}$ , ranges 1.9–2.5%.

Fig. 13 shows that with the same amount of ED bars, the increase of the initial PT force increases the lateral strength of the column models and decreases residual displacement. As the ED bar ratio  $\rho$  increases, the hysteretic energy dissipation increases as well as does residual drift. If the ED bar ratio does not exceed a certain value, the columns exhibit a flag-shaped hysteretic behavior with almost zero residual displacement upon unloading. An optimum ED bar ratio can result in an optimum flag-shaped hysteretic behavior with the unloading branch approaching the abscissa while keeping small residual displacement. Fig. 14a shows the relationship between the equivalent viscous damping and residual displacement for all models. Based on minimizing residual displacement irrespective of aspect ratio or initial PT force, the optimum ED bar ratio  $\rho$  is about 1.2%, corresponding to the optimum equivalent viscous damping of 12–13%. The figure shows that the residual displacement increases significantly when the equivalent viscous damping is larger than 13%. Fig. 14a also shows that with the same ED bar ratio and initial PT force, the column models 7–10 with a high aspect ratio ( $=8$ ) tend to have larger equivalent viscous damping than the column models 3–6 with a low aspect ratio ( $=4$ ). This behavior can be attributed to the fact that the columns with a high aspect ratio have smaller peak strength at the target drift. Fig. 14b shows the ratios of the moment provided by ED bars to the total maximum column moment capacity; this ratio is proportionally dependent on the equivalent viscous damping (or ED bar ratio). To reach the optimum flag-shaped hysteretic behavior, the maximum moment provided by ED bars is about one-quarter of the total column moment based on the equivalent viscous damping of 12–13%.

5. Conclusions

The study of the cyclic performance of unbonded PT precast concrete segmental bridge columns with circular cross section is described in this paper. Longitudinal mild steel bars (ED bars) were

Fig. 14. Equivalent viscous damping versus residual displacement and ED bar moment ratio relationships (6% drift).

Table 4, the aspect ratios of columns are 4.9 and 9.8 with segment diameters of either 500 mm or 1000 mm. The initial PT forces are  $0.25f'_c A_c$  and  $0.35f'_c A_c$ , where  $f'_c = 50$  MPa is the concrete compressive strength and  $A_c$  is the gross area of the concrete section. The

utilized in two specimens and terminated at a certain column height to investigate the effects of anchorage position on the energy dissipation capability and segment joint opening. Two analytical modeling techniques that can capture the response of segmental columns with ED bars were presented. First, the two-plastic-hinge model utilizing the moment–curvature analysis at two segment interfaces was proposed to predict the pushover response of the column. In order to capture the cyclic response of the column, a 2D FE model was developed using one-dimensional truss and beam-column elements. The concrete truss elements were modeled as zero tensile strength and stiffness to capture the gap-opening mechanism at segment interfaces.

Test results show that the ED bar can increase hysteretic energy dissipation, and Specimens 1–3 have equivalent viscous damping of 6.5–8.8%. An equivalent unbonded length along which the strain in the ED bar is assumed uniformly distributed on each of the two sides of the original unbonded length is 5–6 bar diameter. The plastic hinge length in the first or second segments varies with anchorage position of the ED bar and lateral displacement of the column. For Specimens 1 and 3 with larger joint opening and concrete damage at the base than the bottom of the second segment, the plastic hinge length approaches to half the section diameter in the first segment and one-fifth the section diameter in the second segment. However, for Specimen 2 with larger joint opening and concrete damage at the bottom of the second segment than at the base, the plastic hinge length approaches to half the section diameter in these two segments. By comparing the results of pushover analyses using the two-plastic-hinge model to those from the tests, it is evident that given the constant plastic hinge lengths in the bottom two segments the simplified analytical model is capable of predicting the pushover curve, the segment joint opening and the strain in the ED bars.

Although the gap opening predicted by the FE model differs by 30% when compared to the experimental value, the effect of bar anchorage location on the segment gap opening can be captured by this proposed model. Moreover, the peak strength and flag-shaped hysteretic response of the PT column can also be captured by this FE model. Through parametric studies, a higher ED bar ratio results in more hysteretic energy dissipation. If the equivalent viscous damping (or ED bar ratio) is below a certain value, the column exhibits an optimum flag-shaped hysteretic behavior with large hysteretic energy dissipation while keeping small residual displacement upon unloading. The optimum equivalent viscous damping is about 12–13%, corresponding to the optimum ED bar ratio of 1.2%, quite larger than the 0.66% of Specimens 2 and 3. For the columns examined, this amount of ED bars contributes about one-quarter of the total column moment. Note that due to arrangement of ED bars in the circular section, only half of them are effective in dissipating seismic energy in one loading direction.

The plastic hinge lengths determined from the tests are specific to the column details in this study, and experimental work is further needed to assess if the two-plastic-hinge model is applicable to different details of PT concrete segmental columns. Although 2D simplified FE model can reasonably predict the test results, a verification of the 2D model with 3D model, to prove that the difference resulting from the simplification can be ignored, is still needed in the future analysis. Moreover, the effect of tensile strength and stiffness of concrete on the column behavior may also be considered in the analytical model.

## References

- [1] Billington SL, Barnes RW, Breen JE. A precast segmental substructure system for standard bridges. *PCI J* 1999;44(4):56–73.
- [2] Hewes JT. Seismic tests on precast segmental concrete columns with unbonded tendons. *Bridge Struct: Assessment Des Constr* 2007;3(3 & 4):215–27.
- [3] Hewes JT, Priestley MJN. Seismic design and performance of precast concrete segmental bridge columns. Report No. SSRP 2001/25. La Jolla (CA): University of California San Diego; 2002.
- [4] Usami T, Ge H. Ductility of concrete-filled steel box columns under cyclic loading. *J Struct Eng ASCE* 1994;120(7):2021–40.
- [5] Chang KC, Loh CH, Chiu HS, Hwang JS, Cheng CB, Wang JC. Seismic behavior of precast segmental bridge columns and design methodology for applications in Taiwan. Taipei (Taiwan): Area National Expressway Engineering Bureau; 2002 [in Chinese].
- [6] Chou CC, Chen YC. Cyclic tests of post-tensioned precast CFT segmental bridge columns with unbonded strands. *Earthquake Eng Struct Dynam* 2006;35:159–75.
- [7] Kim TH, Lee HM, Kim YJ, Shin HM. Performance assessment of precast concrete segmental bridge columns with a shear resistant connecting structure. *Eng Struct* 2010;32(5):1292–303.
- [8] Chou CC, Hsu CP. Hysteretic model development and seismic response of unbonded post-tensioned precast CFT segmental bridge columns. *Earthquake Eng Struct Dynam* 2008;37:919–34.
- [9] Pampanin S, Priestley MJN, Sriharan S. PRESS phase 3: the five-story precast test building-frame direction response. Report No. SSRP 2000/08. La Jolla (CA): University of California San Diego; 2000.
- [10] Chou CC, Chen JH, Chen YC, Tsai KC. Evaluating performance of post-tensioned steel connections with strands and reduced flange plates. *Earthquake Eng Struct Dynam* 2006;35(9):1167–85.
- [11] Ou YC, Chiewanichakorn M, Aref AJ, Lee GC. Seismic performance of segmental precast unbonded posttensioned concrete bridge columns. *J Struct Eng ASCE* 2007;133(11):1636–47.
- [12] Raynor DJ, Lehman DE, Stanton JF. Bond-slip response of reinforcing bars grouted in ducts. *ACI Struct J* 2002;99(5):568–76.
- [13] Mander JB, Priestley MJN, Park P. Theoretical stress–strain model for reinforced concrete. *J Struct Eng ASCE* 1988;114(8):1804–23.
- [14] Paulay T, Priestley MJN. *Seismic design of reinforced concrete and masonry buildings*. New York: John Wiley & Sons; 1992.
- [15] Chou CC, Tsai KC, Yang WC. Self-centering steel connections with steel bars and a discontinuous composite slab. *Earthquake Eng Struct Dynam* 2009;38:403–22.
- [16] Chou CC, Weng CY, Chen JH. Seismic design and behavior of post-tensioned connections including effects of a composite slab. *Eng Struct* 2008;30:3014–23.
- [17] Chou CC, Chen JH. Column restraint in post-tensioned self-centering moment frames. *Earthquake Eng Struct Dynam* 2010;39(7):751–74.
- [18] Chou CC, Chen JH. Seismic design and shake table tests of a steel post-tensioned self-centering moment frame with a slab accommodating frame expansion. *Earthquake Eng Struct Dynam* 2011;40(11):1241–61.
- [19] Chou CC, Chen YC, Pham DH, Truong VM. Experimental and analytical validation of steel dual-core self-centering braces for seismic-resisting structures. In: 9th International conference on urban earthquake engineering/4th Asia conference on earthquake engineering, Tokyo, Japan; 2012.
- [20] Chang HJ. Seismic effects of energy dissipation bars on post-tensioned precast concrete segmental bridge columns. Chou CC, Liou GS, thesis advisors. Hsinchu (Taiwan): Department of Civil Engineering, National Chiao Tung University; 2009.
- [21] *PCI design handbook: precast and prestressed concrete*, 5th ed. Chicago (IL): Precast/Prestressed Concrete Institute; 1999.
- [22] Priestley MJN, Seible F, Calvi GM. *Seismic design and retrofit of bridges*. New York: John Wiley & Sons, Inc.; 1996.
- [23] Tsai KC, Lin BZ. Development of an object-oriented nonlinear static and dynamic 3D structural analysis program. CEER/R92-04. Taiwan: Center for Earthquake Engineering Research, National Taiwan University; 2003.
- [24] ElGawady MA, Dawood HM. Analysis of segmental piers consisted of concrete filled FRP tubes. *Eng Struct* 2012;38:142–52.
- [25] Chou CC, Chen JH. Analytical model validation and influence of column bases for seismic responses of steel post-tensioned self-centering MRF systems. *Eng Struct* 2011;33(9):2628–43.
- [26] Wang Z, Song W, Wang Y, Wei H. Numerical analytical model for seismic behavior of prestressing concrete bridge column systems. *Eng Struct* 2011;14:2333–40.
- [27] Kunnath SK, Reinhorn AM, Park YJ. Analytical modeling of inelastic seismic response of R/C structures. *J Struct Eng ASCE* 1990;116(4):996–1017.